J Appl Electrochem (2013) 43:159–169
DOI 10.1007/s10800-012-0497-y

ORIGINAL PAPER

# Mesoporous carbons supported non-noble metal Fe–$N_X$ electrocatalysts for PEM fuel cell oxygen reduction reaction

**Alessandro H. A. Monteverde Videla · Lei Zhang · Jenny Kim · Juqin Zeng · Carlotta Francia · Jiujun Zhang · Stefania Specchia**

Received: 17 July 2012 / Accepted: 26 October 2012 / Published online: 7 November 2012


**Abstract** Three types of iron–nitrogen-containing non-noble metal catalysts, supported on an ultrasonic spray pyrolysis mesoporous carbon (USPMC), a hollow core mesoporous shell carbon (HCMSC), and a standard carbon (Ketjen Black CJ600, KB), respectively, are synthesized using a wet-impregnation method. The morphologies and structure as well as composition of the synthesized carbon supports and their corresponding supported Fe–$N_X$ catalysts (namely Fe–$N_X$/USPMC, Fe–$N_X$/HCMSC, and Fe–$N_X$/KB, respectively) are physically characterized using EDX, SEM, FESEM, and BET analysis, respectively. The catalytic activities of these three electrocatalysts toward oxygen reduction reaction (ORR) are measured using rotating disk electrode technique in $O_2$-saturated 0.5 M $H_2SO_4$ solution. The catalyzed ORR exchange current densities are also obtained using the Tafel method based on the measured data. Among these three electrocatalysts, Fe–$N_X$/HCMSC can give the best ORR performance, which is correlated to its higher nitrogen, mesopore, and micropore contents, compared to the other electrocatalysts. It is rationalized that the performance improvement of these electrocatalysts may be achieved as long as an optimal relationship among mesopores, micropores, and even macropores for increasing both ORR kinetics and reactant gases accessibility to the active sites can be found.

**Keywords** Iron–nitrogen electrocatalysts · Fuel cell oxygen reduction reaction · Ultrasonic spray pyrolysis mesoporous carbon · Hollow core mesoporous shell carbon · Microporosity · Mesoporosity

## 1 Introduction

During the last two decades, enormous efforts to introduce and demonstrate polymer electrolyte membrane (PEM) fuel cell technology have been made in terms of both research and development and commercialization. The efficiency of this technology is potentially better than combustion cycle engine for transport applications [1, 2]. However, both the high cost and insufficient durability have hindered its commercialization at current stage. To be competitive in all sectors and to meet consumer requirements, PEM fuel cells will have to be less expensive than they are today, without compromising performance [3]. In the mainstream transportation sector, for example, costs will have to be reduced significantly to compete with internal combustion engines (ICEs), whose costs are actually set at about 30 \$ $kW^{-1}$ for light-duty vehicles [4]. Improvements in the technology have already provided significant cost reductions: in particular, the cost of automotive PEM fuel cells has been reduced by more than 80 % since 2002, reaching a manufacturing cost of about 49 \$ $kW^{-1}$ in 2011 [4]. Although PEM fuel cells are already becoming cost-competitive in a few applications, their further cost reduction is definitely necessary for a widespread commercialization.

Regarding the high cost of PEM fuel cells, the main contributor is associated with the price of their main

A. H. A. Monteverde Videla · J. Zeng · C. Francia · S. Specchia (✉)
Politecnico di Torino, Department of Applied Science and Technology, Corso Duca degli Abruzzi 24, 10129 Turin, Italy
e-mail: stefania.specchia@polito.it

A. H. A. Monteverde Videla · L. Zhang · J. Kim · J. Zhang
National Research Council, Energy, Mining & Environment Portfolio, Government of Canada, 4250 Wesbrook Mall, Vancouver, BC V6T 1W5, Canada
e-mail: lei.zhang@nrc.gc.ca

components, specifically the platinum-based catalysts, which are used for both cathode oxygen reduction reaction (ORR) and anode hydrogen oxidation reaction (HOR) [1, 2]. Therefore, Pt usage reduction [5–11] or using non-noble metal electrocatalysts [12–20] seem to be the promising solution.

In general, the catalyzed ORR kinetics in PEM fuel cells is much slower than that of HOR. Therefore, much more effort has been put into the development of cathode catalysts including both low Pt-containing and non-noble metal catalysts. For a sustainable solution, non-noble metal catalysts may be the targets for research and development because platinum, in fact, still depends on monopolized price suppliers and, in a large-scale scenario, the reserves of this metal are estimated to be not enough for responding to the transportation needs [15]. Regarding non-noble metal electrocatalysts, the most promising ones seem to be heat-treated Fe(II) and/or Co(II) chelates and macrocycles supported on carbon particles [12, 15, 21–30]. The formation of metal−nitrogen ($M–N_X/C$) active centers after the heat treatment is necessary for ORR, as emphasized by the groups of Yeager [24–26] and Dodelet [15, 27, 28]. Regarding the active sites, two types are considered the most active: $M–N_2/C$ and $M–N_4/C$, produced by heat treatment under $NH_3$ atmosphere [15]. As summarized by the group of Dodelet [15, 27, 28], to form ORR active sites, three conditions must exist; (1) nitrogen/metal sources, (2) carbon support, and (3) heat treatment. Regarding the carbon supports, various carbons, such as active carbon, black Pearls 2000 (BP 2000), BP 2000 with pore filler and Vulcan XC-72, have been explored in recent years [15]. Jaouen et al. [27, 28] suggested that the porosity of carbon support particles plays an important role in forming ORR active sites. In this regard, micro- and meso-pores may be more efficient in hosting the active sites. Therefore, exploring new carbon supports which possess unique surface structure and micro-/meso-pores should be one of the approaches in improving the ORR catalytic activity of non-noble metal catalysts.

In this paper, three types of carbon materials, an ultrasonic spray pyrolysis mesoporous carbon (USPMC), a hollow core–mesoporous shell carbon (HCMSC), and a standard carbon (Ketjen Black CJ600), respectively, were employed as catalyst support to prepare iron–nitrogen-containing non-noble metal catalysts. An iron–trypyridyl-*s*-tri-triazine (Fe(II)TPTZ) complex was used as the metal and nitrogen sources, which was deposited by wet-impregnation technique on these three carbon supports, respectively, to form carbon-supported catalyst precursors. Then these precursors were heat-treated at 900 °C in an inert atmosphere to form the final catalysts. Electrochemical measurements using a rotating disk electrode technique were carried out to obtain their corresponding ORR catalytic activities. The catalyzed ORR exchange current densities were obtained using the Tafel method based on the measured data. For a deep understanding, the catalytic ORR activity of these three catalysts were compared according to the carbon supports' structures. The origin of ORR activity was attributed to the formation of $Fe–N_X/C$ active sites [13, 29, 30].

## 2 Experimental section

### 2.1 Chemicals

Nitrogen source as 2,3,5,6-tetrakis(2-pyridyl)pyrazine (TPTZ, 97 %) and metal source as iron(II) acetate (FeAc, 97 %) were purchased from Sigma-Aldrich and Strem Chemicals, respectively, and used as received. Nitrogen and hydrogen gases were supplied in cylinders by Praxair with 99.999 % purity. Isopropanol and ethanol, with 99.5 wt% purity, were purchased from Sigma-Aldrich. Hydrochloric acid solution (1.0 M), and Nafion® alcohol solution containing 5 % Nafion® were purchased from Alpha Aesar. Sulphuric acid with 97–98 wt% purity and Fluoridric acid 5 wt% purity were purchased from Sigma Aldrich. All aqueous solutions were prepared using ultra-pure water obtained from a Millipore Milli-Q system with resistivity >18 $M\Omega\ cm^{-1}$.

### 2.2 Carbon support preparation

In this study, two types of mesoporous carbon (MC) supports were prepared. One MC was prepared by template-assisted ultrasonic spray pyrolysis method, according to the procedure described in one of the patents by the National Research Council of Canada [31]. In the synthesis, an aerosol procedure was used, which enabled to control homogenous powder with spherical solid or hollow particles. Commercially available colloidal silica (50 nm silica solution, LUDOX® TM50, the particle size of colloidal silica templates was chosen according to the carbon surface area and porosity) was used as the template, and sucrose was used as carbon source. Silica and sucrose with a mixing ratio of 3:1 p/p were dissolved in de-ionized water, and stirred for 24 h. Then, hydrochloric acid was added into this mixed solution (pH 1–3) under vigorous stirring. The formed solution, once stabilized, was neutralized as described in the patent [31] in a specific apparatus in which an inert gas flow (Ar) was forced to collect the nanoparticles into gas phase, which was then introduced into the furnace (900 °C) for obtaining the desired nanoparticles. After collecting the nanoparticles, they were washed and dried, followed by a second heat treatment for stabilizing the carbon, and increasing the graphitization level [31].

Finally an acid treatment was performed several times to remove the remaining silica. The so-obtained mesoporous carbon is herein after called USPMC.

The second MC was a HCMSC synthesized using a hard templating method starting from submicrometer-sized solid core–mesoporous shell (SCMS) silica, as described by Zeng et al. [32]. First, the SCMS silica was synthesized using a simultaneous polymerization of tetraethoxysilane (TEOS) and octadecyltrimethoxysilane ($C_{18}$TMS) followed by a removal of organic group, according to the procedure reported by Büchel et al. [33]. The SCMS silica material was then retrieved by centrifugation and further calcined at 550 °C for 6 h under oxygen atmosphere. Then, the HCMSC was synthesized using a hard templating method starting from the previously prepared SCMS silica and sucrose in a $H_2SO_4$ solution. The carbon–silica composite was obtained after pyrolysis at 900 °C for 6 h, and then washed in 5 wt% HF solution to remove silica template [34]. The detailed preparation procedure was reported in the paper of Zeng et al. [32]. The second MC is herein later called HCMSC.

The third support was a commercial carbon, namely the Ketjen Black CJ600 purchased from Cabot Corporation, herein after called KB.

### 2.3 Preparation of the Fe–$N_X$/C electrocatalysts

For the preparation of the Fe(II)TPTZ complex solution, a 1:6 mol ratio of Fe to TPTZ was used. To avoid the formation of Fe(III), pH near 1 was used, where Fe(II) is very stable, preventing the hydrolysis reaction; the reaction was carried out in a glove-box under argon atmosphere. The synthesis was initiated by adding a 0.018 M Fe(II) acetate aqueous solution into a 0.132 M TPTZ, 0.4 M HCl solution under constant stirring for 2 h to form a blue precursor complex solution of Fe(II)TPTZ. After that, according to a desired Fe content of 5 wt%, this precursor complex solution was added drop by drop into a carbon-support suspension made of carbon in 3 wt% ethanol aqueous solution under constant stirring for at least 20 h. The resulting mixture was then dried in an oven at 90 °C overnight, yielding a black powder of carbon-supported Fe(II)TPTZ (Fe(II)TPTZ/C). The obtained Fe(II)TPTZ/C powder was grounded in a mortar and then weighted and placed in a Thermcraft tube furnace under $N_2$ flow at a rate of 150 NmL $min^{-1}$ for 2 h at room temperature to remove any residual air. The pyrolysis process of Fe(II)TPTZ/C was carried out in this tube furnace by increasing the temperature with a ramping rate of 5 °C $min^{-1}$ until the desired heat-treatment temperature of 900 °C was reached. The furnace was then held at this temperature for 2 h, followed by a cooling process at a rate of 5 °C $min^{-1}$ until room temperature. The electrocatalysts thus obtained were grounded again before their use for the physical characterization and electrochemical measurements. The electrocatalysts are herein after called Fe–$N_X$/USPMC, Fe–$N_X$/HCMSC, and Fe–$N_X$/KB, respectively.

### 2.4 Physical characterization of the Fe–$N_X$/C electrocatalysts

The morphologies of the prepared mesoporous carbon samples were examined using a FEI inspect S50/EDAX. Field emission scanning electron microscope (FESEM; model JEOL JSM 6700F) was also employed to determine the surface morphologies and sphere sizes.

Nitrogen adsorption isotherms at 77 K were recorded by an ASAP2010 Instrument (Micromeritics). The specific surface area (SSA) of the samples was calculated using the Brunauer–Emmett–Teller (BET) method within the relative pressure range of 0.05–0.2 [35]. The pore-size distribution (PSD) was obtained with the Barrett–Joyner–Halenda (BJH) method calibrated for cylindrical pores according to the improved Kruk–Jaroniec–Sayari (KJS) method [36].

X-ray photoelectron spectroscopy (XPS) measurements were carried out on Fe–$N_X$/C samples using a Physical Electronics PHI 5800 (USA) multi-technique ESCA system (with monochromatic Al-Kα X-ray radiation). The survey and narrow spectra were obtained under identical conditions and a charging correction with reference to C 1 s at 284.5 eV [37], during which the samples were placed in an ultrahigh vacuum chamber at $2 \times 10^{-10}$ Torr. Multipak 9.0 software was used for obtaining semi-quantitative atomic percentage compositions.

### 2.5 Electrochemical characterization of the Fe–$N_X$/C electrocatalysts

The electrocatalytic ORR activities of electrocatalysts prepared were evaluated in a three-electrode electrochemical cell using a Pine-Instrument's Bipotentiostat AFCBP1, equipped with a speed rotator. A catalyst-coated glassy carbon disk electrode with a geometric area of 0.2 $cm^2$ was used as the working electrode, a platinum wire was used as the counter electrode, and a dynamic hydrogen electrode (DHE) as the reference electrode, respectively. Linear sweep voltammetry (LSV) was performed at room temperature in $O_2$-saturated 0.5 M $H_2SO_4$ solution at room temperatures. ORR current–voltage curves were recorded at a scan rate of 10 mV $s^{-1}$ under various electrode rotation rates (100, 200, 400, 900, and 1,600 rpm, respectively). Oxygen was bubbled directly into the cell for at least 30 min before the test and was flushed over the cell solution during the measurement. On the working electrode surface, a uniform catalyst layer containing 450 μg $cm^{-2}$

of Fe–$N_X$/C catalyst and 0.22 μg $cm^{-2}$ of Nafion® ionomer was coated. In prepare the catalyst ink, 4 mg of catalyst were ultrasonically dispersed in 1 mL of ethanol to form a catalyst suspension.

## 3 Results and discussion

### 3.1 Physical characterization of carbon supports and their corresponding Fe–$N_X$/C electrocatalysts

Nitrogen sorption isotherms and SEM photos were used as morphology characterization of the prepared two mesoporous carbons, one is USPMC, and the other is HCMSC. Figure 1 shows the morphological structures of the prepared carbon samples. As shown in Fig. 1a, b, the spherical structure of the carbon particles in the USPMC sample can be seen with the presence of pores. The diameters of these pores are ranging from mesoporous to the microporous region, respectively. The carbon sphere particles range from 400 nm to 4 μm. Such a high porosity could benefit the diffusion of reactants during the electrochemical reactions. Figure 1c, d enlightens the spherical and uniform shape of the carbon particles in the HCMSC sample, with a uniform carbon particle distribution (approximately 400 nm in particles size). The FESEM image (Fig. 1d) confirms that the HCMSC has a hollow-core diameter of approximately 300 nm and shell thickness of ~50 nm.

Nitrogen adsorption–desorption isotherms for both USPMC and HCMSC samples are shown in Fig. 2a, which can be classified as a Type IV isotherm with $H_2$-type hysteresis according to the International Union of Pure and Applied Chemistry nomenclature. The carbon support (USPMC) prepared by USP technique presented a much higher hysteresis loop, sign of the presence of a higher mesoporous volume compared to the HCMSC support. This is even supported by the pore-size distribution (PSD) of these two carbon supports, as reported in Fig. 2b. Surface structural parameters for both the USPMC and HCMSC samples are summarized in Table 1. The structural data belonging to the commercial support KB were taken from the open literature [38, 39]. The USPMC carbon exhibits a larger-specific surface area (SSA) and total pore volume ($V_{total}$), which is mainly attributed to the presence of mesopores in the spherical carbon particles, as evidenced in Fig. 1b. In addition, it is worthwhile to note that the carbon capsule of the HCMSC sample has a bimodal pore system composed of a spherical macroporous core and mesopores in the shell connecting inside and outside of the hollow core when micropores are present. The commercial carbon KB presented the lower specific surface area and the lower total pore volume.

For catalyst characterization, the presence of nitrogen in the samples and the interaction between carbon support and iron were determined by XPS. Nitrogen doping has been an effective way to tailor the properties of carbon support and render its potential use for various applications. There are several nitrogen functional groups in nitrogen-doped carbon. In particular, four types of nitrogen functional groups were described at different binding energies such as: pyridinic N at 398.3–398.8 eV (N1), pyrrolic and/or cyanide-like N at 400.0–400.7 eV (N2), quaternary graphite-like N at 401.0–401.6 eV (N3) and N oxides, nitro or nitrous groups, of pyridine at 404.9 eV (N4) [40–44]. The role of the real "electrocatalytically active sites" is still controversial since their contribution to the catalytic activity is not well defined. In some studies, the enhanced electrocatalytic activity was attributed to pyridinic-N (N1) and/or pyrrolic-N (N2) [45, 46]. On the contrary, recent studies suggested that graphitic nitrogen (N3) is more important for the electrocatalytic activity of nitrogen-doped carbon [47, 48].

The N1s XPS spectra are shown in Fig. 3 for the three prepared electrocatalysts, Fe–$N_X$/USPMC, Fe–$N_X$/HCMSC, and Fe–$N_X$/KB, respectively, where the peaks intensities were normalized for all samples. The Fe–$N_X$/HCMSC sample (Fig. 3b) presents the higher nitrogen–carbon ratio, suggesting that the nitrogen fixation depends on the pore diameter and the structure of the material. The Nitrogen contents for all samples are reported in Table 2. The lower quantity of pyridinic-N (N1) in the Fe–$N_X$/USPMC and Fe–$N_X$/KB electrocatalysts could be attributed to conversion into pyrrolic-N (N2) and pyridine-N-oxides (N4), whose values are higher compared to those of the Fe–$N_X$/HCMSC electrocatalyst, during the pyrolysis temperature. The Fe–$N_X$/HCMSC electrocatalyst, instead, presents the highest amount of pyridinic-N (N1), which should be the most active specie for ORR [45, 46]. According to the finding of Dodelet's group [15, 27, 28], the pyridinic-N (N1) is usually present in micropores, which are in this case present in the Fe–$N_X$/HCMSC electrocatalysts, but not in the Fe–$N_X$/USPMC one.

The pyridinic-N group (N1) is bonded to two carbon atoms in the carbon plane with a basic lone pair of electrons. This is associated with the formation of active sites Fe–$N_{2+2}$, recognized as the active site, which are probably formed on the edge of a graphitized carbon [49–51]. At the same synthesis conditions, Fe–$N_X$/HCMSC presents a better nitrogen fixation than both the Fe–$N_X$/USPMC and Fe–$N_X$/KB electrocatalysts. This could be attributed to the presence of microporous particles, as described by Lefèvre et al. [15]. The presence of high quantities of N oxides of pyridine (N4) in the cases of both Fe–$N_X$/USPMC and Fe–$N_X$/KB, could be attributed to a less protonation reaction, which can be related to a mayor stability in acid atmosphere [49].

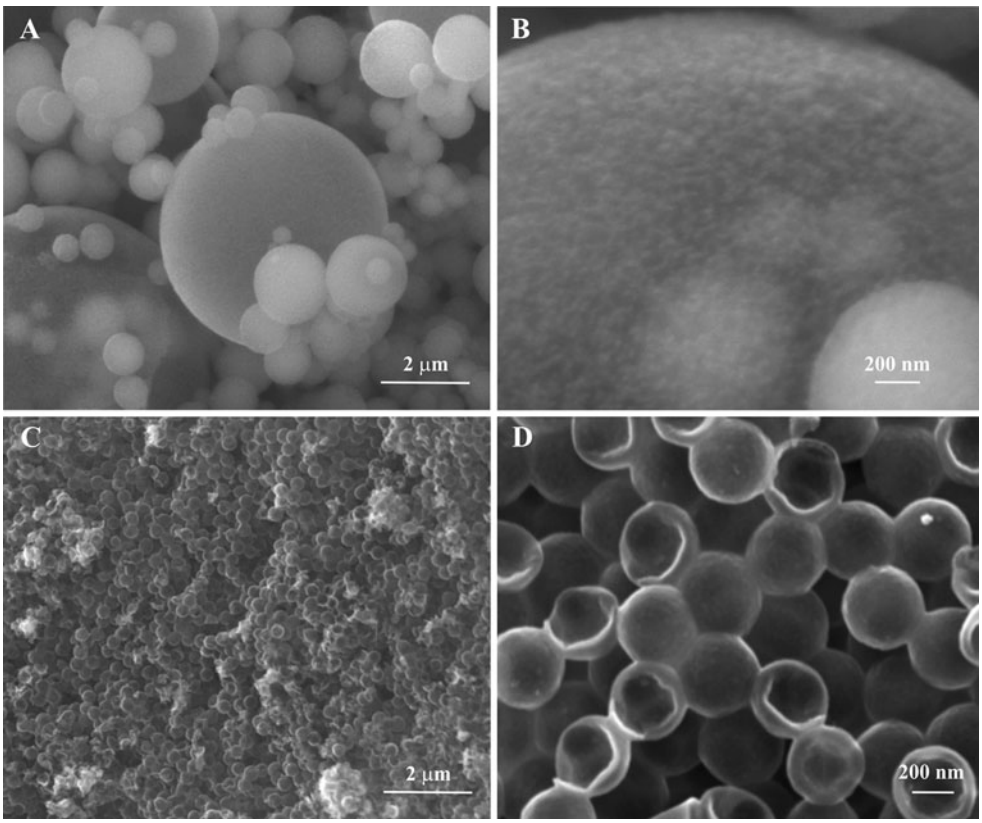


**Fig. 1** SEM (**a**, **c**) and FESEM (**b**, **d**) images of USPMC (**a**, **b**) and HCMSC (**c**, **d**) samples

### 3.2 Electrochemical characterization of Fe–$N_X$/C electrocatalysts

The electrocatalytic ORR activities of the prepared electrocatalysts were investigated using rotating disk electrode technique (RDE). Figure 4 shows the current–voltage (*I–V*) curves obtained using Fe–$N_X$/USPMC, Fe–$N_X$/HCMSC, and Fe–$N_X$/KB as catalysts in $O_2$-saturated 0.5 M $H_2SO_4$ solution, respectively. Through the analysis of the curves, the obtained results are summarized in Table 3. It can be seen that the oxygen reduction potentials ($E_{ORP}$) can be correlated to the quantity of nitrogen, that is, the more the catalyst contains nitrogen, the more positive the $E_{ORP}$ potential would be. The analysis at different voltages, specifically in the kinetic region (0.8 V vs. RHE) and in the diffusion control region (0.3 V vs. RHE) is also summarized in Table 3. Compared to KB carbon support, both mesoporous carbons can give high ORR activities. As previously mentioned, for obtaining a high catalytic activity, the presence of microporous is necessary to host nitrogen, and the presence of mesopores is also necessary for assuring a good diffusion interaction [52, 53]. These can be used to explain why mesoporous carbon supports can give high ORR performance when compared to that of non-mesoporous carbon-like KB.

For ORR mechanism understanding, Koutecky–Levich (K–L) theory [54] was used to obtain the overall ORR electron transfer numbers based on the data in Fig. 4, according to Eq. (1):

$$\frac{1}{I} = \frac{1}{I_k} + \frac{1}{I_{lev}} \tag{1}$$

where $I$ is the measured current density, $I_k$ is the kinetic current density, and $I_{lev}$ is the Levich current density. $I_k$ can be expressed as Eq. (2):

$$I_k = nFAK_{O_2}C_{O_2}\Gamma_{catalyst} \tag{2}$$

where $n$ is the overall electron transfer number, $A$ is the electrode area, $K_{O_2}$ is the kinetic constant of ORR, $C_{O_2}$ is the concentration of dissolved $O_2$, $\Gamma_{catalyst}$ is the surface concentration of the catalyst, or the catalyst loading, and $F$ is the Faraday's constant. $I_{lev}$ can be expressed as Eq. (3):

$$I_{lev} = 0.201nFAC_{O_2}D_{O_2}^{2/3}v^{-1/6}\omega^{1/2} \tag{3}$$

where $D_{O_2}$ is the diffusion coefficient of $O_2$, $v$ is the kinetic viscosity of the electrolyte solution, and ω is the electrode rotation rate with a unit of rpm. According to Eqs. (1–3), the kinetic current density and the overall ORR electron transfer number if the values of $C_{O_2}$, $D_{O_2}$, and $v$ are known, could be obtained.

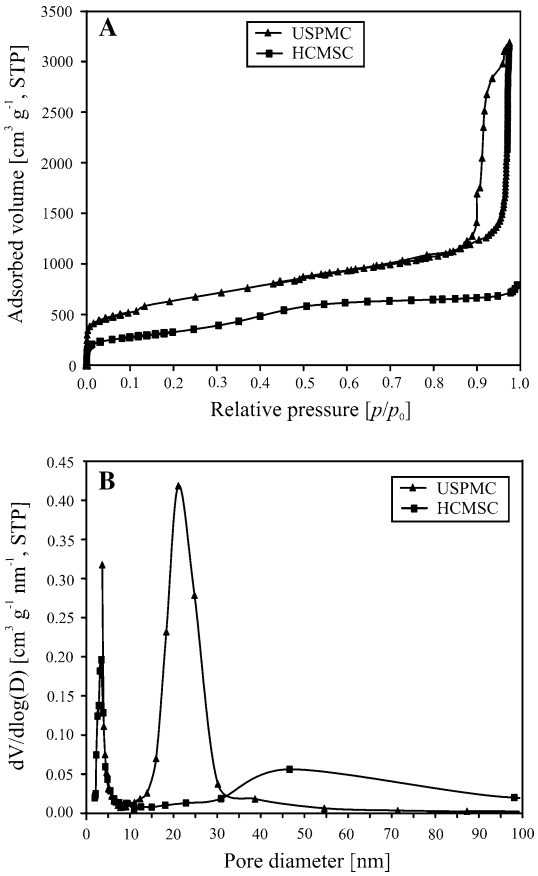


**Fig. 2** $N_2$ adsorption/desorption isotherms (**a**) and particle-size distribution (**b**) of USPMC and HCMSC samples

**Table 1** Surface characterization of carbon supports from BET and BJH analysis (data of KB taken from references [38, 39])

| | SSA ($m^2$ $g^{-1}$) | $D_{BJH}$ (nm) | $V_{total}$ ($cm^3$ $g^{-1}$) | $V_{micro}$ ($cm^3$ $g^{-1}$) |
|---|---|---|---|---|
| USPMC | 2,124 | 21.1 | 4.3 | – |
| HCMSC | 1,187 | 3.5 | 1.1 | 0.20 |
| KB [38, 39] | 1,400 | – | 0.75 | 0.64 |

By observing Fig. 4, it is worth noting that the curves of current densities belonging to all catalysts do not reach steady state conditions in the diffusion limiting current regime at any rotational speed. Theoretically, according to the K–L theory, the calculation of the ORR electrons *n* is possible only in the diffusion limiting current regime. Practically, it is possible to calculate the overall electron number based on slope of the K–L plot at any mixed potential as long as the current is a mixed between kinetic and diffusion currents, as even reported by various authors in the literature [55–60], even if it may be more accurate when the potential used is located in the diffusion current range at which the diffusion current is dominating. Thus,

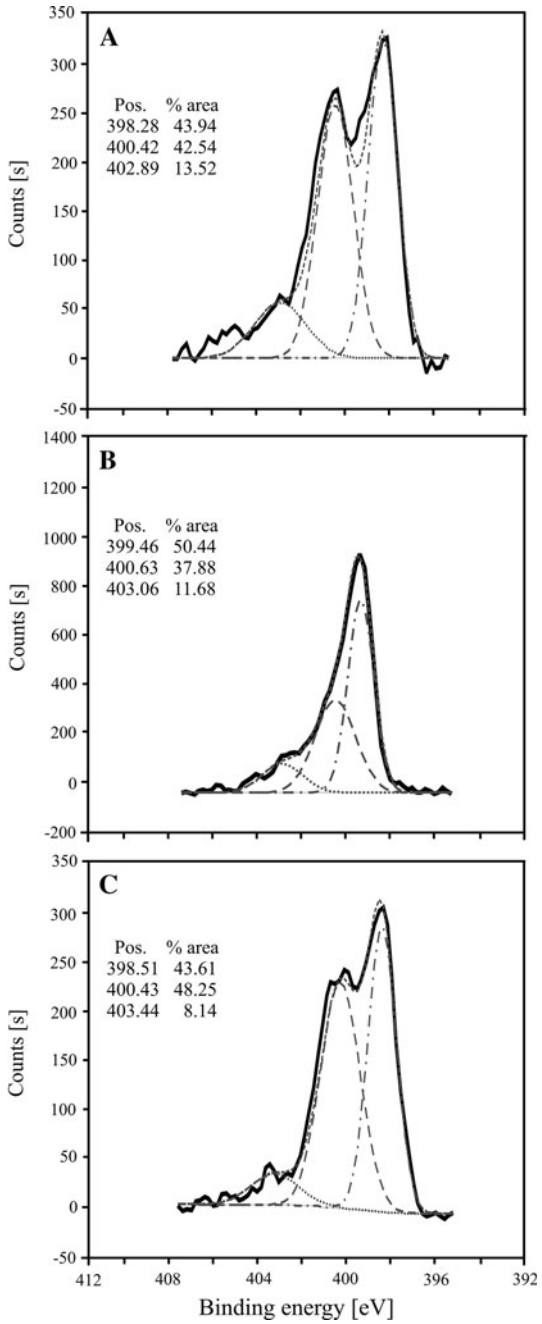


**Fig. 3** Deconvolution of XPS N1s spectra for Fe–$N_X$/USPMC (**a**), Fe–$N_X$/HCMSC (**b**), and Fe–$N_X$/KB (**c**) electrocatalysts, respectively

the calculation of the electron number was performed by analyzing the slopes of the K–L plots at different voltages, specifically at 0.1, 0.2, 0.3, 0.4, and 0.5 V, respectively, and by verifying that the calculated slopes were almost constant for all considered potential values (K–L plots almost parallel straight lines, not reported here for sake of simplicity, with slope variations in the order of ±0.05 for all catalysts, within the fitting errors). The calculated slopes for each catalyst were used to determine the number of electrons, as reported in Table 3.

**Table 2** Nitrogen contents, relative intensities, and binding energies of N1s peaks from XPS analysis

| | Total N (wt%) | XPS analysis (wt%) | | | | Binding energy (eV) | | |
|---|---|---|---|---|---|---|---|---|
| | N | N1 | N2 | N3 | N4 | N1 | N2 | N4 |
| Fe–$N_X$/USPMC | 6.3 | 43.9 | 42.6 | 0 | 13.5 | 398.28 | 400.42 | 402.89 |
| Fe–$N_X$/HCMSC | 11.7 | 50.4 | 37.9 | 0 | 11.7 | 399.46 | 400.63 | 403.06 |
| Fe–$N_X$/KB | 5.4 | 43.6 | 48.3 | 0 | 8.1 | 398.51 | 400.43 | 403.44 |

N1: pyridinic N; N2: pyrrolic and/or cyanide-like N; N3: quaternary graphite-like N; N4: N oxides, nitro, or nitrous groups, of pyridine

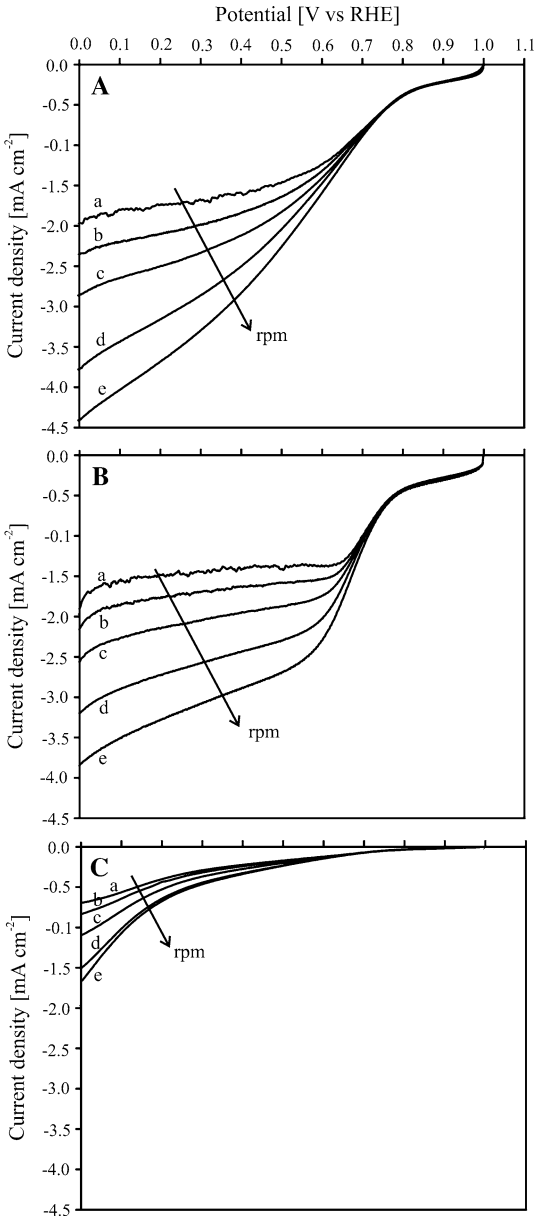


**Fig. 4** Current–voltage curves for oxygen reduction reaction catalyzed by Fe–$N_X$/USPMC (**a**), Fe–$N_X$/HCMSC (**b**), and Fe–$N_X$/KB (**c**) electrocatalysts, respectively, in $O_2$-saturated 0.5 M $H_2SO_4$ solution. Electrode rotation rates at 100 rpm (*a*), 200 rpm (*b*), 400 rpm (*c*), 900 rpm (*d*), and 1,600 rpm (*e*), respectively. Potential scan rate: 10 mV $s^{-1}$. Catalyst loadings: 450 μg $cm^{-2}$ for each sample, respectively

Normally, for a fuel cell application, the optimal pathway should be four electrons from $O_2$ to $H_2O$, avoiding the formation of peroxide. From Table 3, it can be seen that the catalyst made with the commercial carbon support, Fe–$N_X$/KB, only gives a pathway very close to two electrons, while both Fe–$N_X$/USPMC and Fe–$N_X$/HCMSC can give a four-electron transfer process. This may be caused by the obstruction of both mesopores and micropores in KB, producing less accessible active sites for ORR [53]. The highest activity belonged to the Fe–$N_X$/HCMSC electrocatalyst which contains much more micropores, mesopores, and even macropores. Here, macropores are believed to be necessary for letting the oxygen diffusing and adsorbing on the surface, thus increasing the mass transfer capabilities, as shown by the limiting currents of Fe–$N_X$/HCMSC. Therefore, the performance improvement of these electrocatalysts could be obtained by finding out an optimal relationship among meso-, micro-, and macro-pores, and also the reactant gases accessibility to the active sites [39].

### 3.3 Electrochemical kinetic analysis for the ORR catalyzed by Fe–$N_X$/C electrocatalysts

To obtain the electrochemical kinetic parameters of the ORR catalyzed by Fe–$N_X$/C electrocatalysts, the RDE current–potential curves were also analyzed by the Tafel method [54]. From Fig. 4 it can be seen that in the potential range of 0.7–0.8 V versus RHE, the measured current density (*I*) for the ORR is almost independent of the electrode rotation rate, suggesting that the current densities in this narrow potential (or low overpotential) range are purely electrochemical kinetic current densities. However, when the potential is less than 0.7 V, the current density becomes dependent on the electrode rotation rate, suggesting that the current densities in the potential range <0.7 V are affected by both electrochemical kinetic and oxygen diffusion currents. For a cathodic reaction, the relationship between the electrode potential and the current density in the low overpotential range (i.e., 0.7–0.8 V) can be expressed as a Tafel form, Eq. (4):

$$E = E^0 + \frac{2.303RT}{\alpha nF}\log\left(I^0\right) - \frac{2.303RT}{\alpha nF}\log(I) \qquad (4)$$

where *E* is the electrode potential, $E^0$ is the thermodynamic electrode potential of the ORR (1.23 V vs. SHE), *R* is the

**Table 3** Electrochemical characterization of the prepared electrocatalysts via RHE technique

| | Total N (wt%) | $E_{ORP}$ (vs. RHE) | Current density (mA cm$^{-2}$) | | ORR electron transfer number $n$ K–L electrons |
|---|---|---|---|---|---|
| | | | at 0.8 V | at 0.3 V | |
| Fe–$N_X$/USPMC | 6.3 | 0.81 | −0.3816 | −3.2926 | 3.2 |
| Fe–$N_X$/HCMSC | 11.7 | 0.89 | −0.9980 | −3.9898 | 3.8 |
| Fe–$N_X$/KB | 5.4 | 0.71 | −0.0405 | −0.4701 | 2.3 |

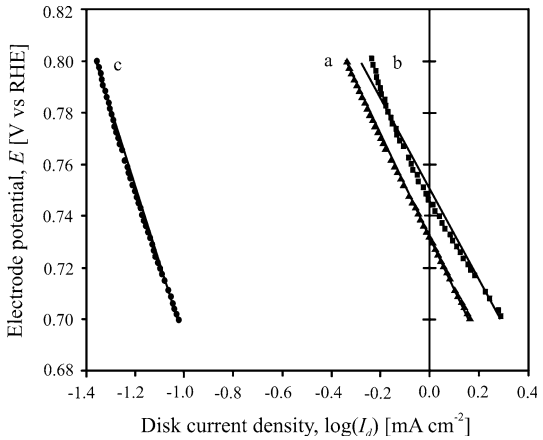


**Fig. 5** Tafel plots for oxygen reduction reaction catalyzed by Fe–$N_X$/USPMC (*a*), Fe–$N_X$/HCMSC (*b*), and Fe–$N_X$/KB (*c*) electrocatalysts, respectively, according to Eq. (4). Data from Fig. 4

universal gas constant (8.314 J mol$^{-1}$ K$^{-1}$), $T$ is the working temperature (K), $F$ is the Faraday constant (96,487 C mol$^{-1}$), $n$ and $\alpha$ are, respectively, the electron transfer number and coefficient in the rate-determining step (RDS) of the catalyzed ORR, respectively, $I^0$ is the exchange current density of the catalyzed ORR, and $I$ is the measured disk current density. According to Eq. (4), the plot of $E$ versus log($I$) allows calculating the Tafel slope ($2.303RT/\alpha nF$), and an intercept $\left(E^0 + \frac{2.303RT}{\alpha nF}\log(I^0)\right)$, as shown in Fig. 5. Thus, from the slopes and intercepts obtained for the different Fe–$N_X$/C catalysts in the low current density ranges (kinetic ranges), both the $\alpha$ and $I^0$ values were calculated according to Eq. (4), and the obtained values are listed in Table 4 for the different Fe–$N_X$/C catalysts. The calculations were carried out in the oxygen reduction potential region ($E_{ORP}$), defined previously as a basic line for obtain the kinetic parameters. The maximum exchange current density belongs to the Fe–$N_X$/HCMSC electrocatalyst. This result confirms that the presence of a higher quantity of micro-, meso-, and macropores in the structure of the carbon support is favorable in enhancing the electrocatalytic activity of the catalysts toward ORR, as previously pointed out.

From the value of $I^0$, the kinetic rate constant (or electron transfer rate constant) in the RDS, $k_e$, can also be obtained using the relationship $I^0 = nFk_eC_{O_2}$ (where the value of the overall electron transfer number, $n$, is taken from the K–L plot, as previously reported in Table 3). The obtained values are also listed in Table 4: they are in agreement with what previously observed, further confirming that the Fe–$N_X$/HCMSC electrocatalyst can yield the best ORR catalytic activity.

Theoretically, a Tafel slope of 120 mV dec$^{-1}$ is due to the rate-determining step associated with the first-electron transfer, while a Tafel slope of 60 mV dec$^{-1}$ has been explained in the literature as the migration rate of adsorbed oxygen intermediates with a Temkin isotherm [61, 62]. In this case, Tafel slopes of 131, 180, and 270 mV dec$^{-1}$ were obtained for Fe–$N_X$/HCMSC, Fe–$N_X$/USPMC, and Fe–$N_X$/KB, respectively. Higher Tafel slopes, as in the case of the electrocatalyst supported on the commercial Ketjen Black (KB), may result from the presence of surface redox couples/functional groups which act as a barrier for the oxygen evolution [62]. Tafel curves and kinetic parameters (see Fig. 5; Table 4) showed that a support having a higher mix of micro- and meso-pores could effectively suppress the adsorption of hydroxy species, leading to both higher electron transfer coefficient and exchange current density [63, 64].

**Table 4** Summary of the electron transfer coefficient $\alpha$ (assuming the electron transfer number $n$ in the ORR rate-determining step equal to 1), the exchange current density $I^0$, and the electron transfer rate constant $k_e$ for the Fe–$N_X$/C electrocatalysts (electrolyte: $O_2$-saturated 0.5 M $H_2SO_4$ solution; catalyst loading in the electrode coating layer: 450 μg cm$^{-2}$ for each sample; temperature: 25 °C, pressure 1 atm)

| | $\alpha$ | $I^0$ (A cm$^{-2}$) | $k_e$ (cm s$^{-1}$) |
|---|---|---|---|
| Fe–$N_X$/USPMC | 0.32 | 1.84E−06 | 5.08E−06 |
| Fe–$N_X$/HCMSC | 0.43 | 2.78E−07 | 6.48E−07 |
| Fe–$N_X$/KB | 0.21 | 1.16E−06 | 4.48E−06 |

The obtained results are very promising, and it is expected that the performance of the synthesized electrocatalysts in terms of fuel cell performance should be relatively good. The understanding of the graphitization, studying mechanism of reactions, and the transition metal state will be a next fundamental step to turn these catalysts competitive as much as platinum in low temperature fuel cell applications in a near future.

## 4 Conclusions

In this study, three types of iron–nitrogen-containing non-noble metal catalysts, supported on an USPMC, a HCMSC,

and a standard carbon (Ketjen Black CJ600, KB), respectively, were synthesized using a wet-impregnation method. The morphologies and structure as well as composition of the synthesized carbon supports and their corresponding supported Fe–$N_X$ electrocatalysts (namely Fe–$N_X$/HCMSC, Fe–$N_X$/USPMC, and Fe–$N_X$/KB, respectively) were physically characterized by EDX, SEM, FESEM, and BET analysis, respectively. The catalytic activities toward ORR were tested using rotating disk electrode technique in $O_2$-saturated 0.5 M $H_2SO_4$ solution. The obtained ORR performance and reaction kinetic results were compared: the HCMSC supported Fe–$N_X$ electrocatalyst (Fe–$N_X$/HCMSC) gave the best ORR activity and also catalyzed a four-electron transfer process from $O_2$ to $H_2O$. This could be explained according to the contents of nitrogen, meso-, and micro-pores present in the catalyst carbon support. In Fe–$N_X$/HCMSC, the contents of nitrogen, meso-, and micro-pores are higher than other two, giving higher ORR activity. The slopes of Tafel plots suggest that the first-electron transfer is the reaction rate-determining step of the catalyzed ORR and that a support having a higher mix of micro- and meso-pores could effectively suppress the adsorption of hydroxy species, leading to higher electron transfer coefficient and exchange current density.

Therefore, it is rationalized that the presence of both micropores and mesopores is necessary to obtain a good catalytic activity toward ORR. Furthermore, the performance improvement of these electrocatalysts could be achieved by finding out an optimal relationship among meso-, micro-, and even macro-pores for increasing both ORR kinetics and reactant gases accessibility to the active sites.

**Acknowledgments** Dr Edvige Celasco and Mr Mauro Raimondo from Politecnico di Torino are gratefully acknowledged for SEM/XPS analysis. The authors express their gratitude and recognition to Dr Brian McLernon from National Research Council of Canada and Prof. Paolo Spinelli from Politecnico di Torino for the valuable and fruitful discussions.

## References

1. Wu G, More KL, Johnston CM, Zelenay P (2011) High-performance electrocatalysts for oxygen reduction derived from polyaniline, iron, and cobalt. Science 332:443–447
2. Specchia S, Francia C, Spinelli P (2011) Polymer electrolyte membrane fuel cells. In: Electrochemical technologies for energy storage and conversion, 1st edn. Wiley-VHC, Weinheim, pp 601–670
3. Ohma A, Mashio T, Sato K, Iden H, Ono Y, Sakai K, Akizuki K, Takaichi S, Shinohara K (2011) Analysis of proton exchange membrane fuel cell catalyst layers for reduction of platinum loading at Nissan. Electrochim Acta 56:10832–10841
4. The Department of Energy, Hydrogen and Fuel Cells Program Plan (2011) An integrated strategic plan for the research, development, and demonstration of hydrogen and fuel cell technologies. www.hydrogen.energy.gov/pdfs/program_plan2011.pdf. Accessed 12 July 2012
5. Chen ZW, Waje M, Li WZ, Yan YS (2007) Supportless Pt and PtPd nanotubes as electrocatalysts for oxygen-reduction reactions. Angew Chem Int Ed 46:4060–4063
6. Ramaswamy N, Arruda TM, Wen W, Hakim N, Saha M, Gullá A, Mukerjee S (2009) Enhanced activity and interfacial durability study of ultra low Pt based electrocatalysts prepared by ion beam assisted deposition (IBAD) method. Electrochim Acta 54:6756–6766
7. Liao MJ, Wei ZD, Chen SG, Li L, Ji MB, Wang YQ (2010) Ultra low Pt-loading electrode prepared by displacement of electrodeposited Cu particles on a porous carbon electrode. Int J Hydrogen Energy 35:8071–8079
8. Esmaeilifar A, Rowshanzamir S, Eikani MH, Ghazanfari E (2010) Synthesis methods of low-Pt-loading electrocatalysts for proton exchange membrane fuel cell systems. Energy 35:3941–3957
9. Sebastián D, Lázaro MJ, Suelves I, Moliner R, Baglio V, Stassi A, Aricò AS (2012) The influence of carbon nanofiber support properties on the oxygen reduction behavior in proton conducting electrolyte-based direct methanol fuel cells. Int J Hydrogen Energy 37:6253–6260
10. Zeng J, Francia C, Dumitrescu MA, Monteverde Videla AHA, Ijeri VS, Specchia S, Spinelli P (2012) Electrochemical performance of Pt-based catalysts supported on different ordered mesoporous carbons (Pt/OMCs) for oxygen reduction reaction. Ind Eng Chem Res 51:7500–7509
11. Sebastián D, García Ruíz A, Suelves I, Moliner R, Lázaro MJ, Baglio V, Stassi A, Aricò AS (2012) Enhanced oxygen reduction activity and durability of Pt catalysts supported on carbon nanofibers. Appl Catal B: Environ 115–116:269–275
12. Chen ZW, Higgins DC, Yu A, Zhang L, Zhang J (2011) A review on non-precious metal electrocatalysts for PEM fuel cells. Energy Environ Sci 4:3167–3192
13. Wang L, Zhang L, Zhang J (2011) Improved ORR activity of non-noble metal electrocatalysts by increasing ligand and metal ratio in synthetic complex. Electrochim Acta 56:5488–5492
14. Oh HS, Kim H (2012) The role of transition metals in non-precious nitrogen-modified carbon-based electrocatalysts for oxygen reduction reaction. J Power Sources 212:220–225
15. Lefèvre M, Proietti E, Jaouen F, Dodelet JP (2009) Iron-based catalysts with improved oxygen reduction activity in polymer electrolyte fuel cells. Science 324:71–74
16. Liu H, Song C, Tang Y, Zhang J, Zhang J (2007) High-surface-area CoTMPP/C synthesized by ultrasonic spray pyrolysis for PEM fuel cell electrocatalysts. Electrochim Acta 52:4532–4538
17. Chen Z, Higgins DC, Chen ZW (2010) Electrocatalytic activity of nitrogen doped carbon nanotubes with different morphologies for oxygen reduction reaction. Electrochim Acta 55:4799–4804
18. Chen Z, Higgins DC, Chen ZW (2010) Nitrogen doped carbon nanotubes and their impact on the oxygen reduction reaction in fuel cells. Carbon 48:3057–3065
19. Choi J, Higgins DC, Chen ZW (2011) Highly durable graphene nanosheet supported iron catalyst for oxygen reduction reaction in PEM fuel cells. J Electrochem Soc 159:B87–B90
20. Higgins DC, Chen Z, Chen ZW (2011) Nitrogen doped carbon nanotubes synthesized from aliphatic diamines for oxygen reduction reaction. Electrochim Acta 56:1570–1575
21. Collman JP, Marrocco M, Denisevich P, Koval C, Anson FC (1979) Potent catalysis of the electroreduction of oxygen to water by dicobalt porphyrin dimers adsorbed on graphite electrodes. J Electroanal Chem Interfacial Electrochem 101:117–122
22. Collman JP, Denisevich P, Konai Y, Marrocco M, Koval C, Anson FC (1980) Electrode catalysis of the four-electron reduction of oxygen to water by dicobalt face-to-face porphyrins. J Am Chem Soc 102:6027–6036
23. Liu HY, Weaver MJ, Wang CB, Chang CK (1983) Dependence of electrocatalysis for oxygen reduction by adsorbed dicobalt

cofacial porphyrins upon catalyst structure. J Electroanal Chem Interfacial Electrochem 145:439–447
24. Yeager EB (1984) Electrocatalysts for $O_2$ reduction. Electrochim Acta 29:1527–1537
25. Scherson D, Tanaka AA, Gupta SL, Tryk D, Fierro C, Holze R, Yeager EB (1986) Transition metal macrocycles supported on high area carbon: pyrolysis—mass spectrometry studies. Electrochim Acta 31:1247–1258
26. Morcos I, Yeager EB (1970) Kinetic studies of the oxygen–peroxide couple on pyrolytic graphite. Electrochim Acta 15:953–975
27. Jaouen F, Lefèvre M, Dodelet JP, Cai M (2006) Heat-treated Fe/N/C catalysts for $O_2$ electroreduction: are active sites hosted in micropores? J Phys Chem B 110:5553–5558
28. Jaouen F, Proietti E, Lefèvre M, Chenitz R, Dodelet JP, Wu G, Chung HT, Johnston CM, Zelenay P (2011) Recent advances in non-precious metal catalysis for oxygen-reduction reaction in polymer electrolyte fuel cells. Energy Environ Sci 4:114–130
29. Velázquez-Palenzuela A, Zhang L, Wang L, Cabot PL, Brillas E, Tsay K, Zhang J (2011) Fe–$N_x$/C electrocatalysts synthesized by pyrolysis of Fe(II)–2,3,5,6-tetra(2-pyridyl)pyrazine complex for PEM fuel cell oxygen reduction reaction. Electrochim Acta 56:4744–4752
30. Li S, Zhang L, Liu H, Pan M, Zan L, Zhang J (2010) Heat-treated cobalt–tripyridyl triazine (Co–TPTZ) electrocatalysts for oxygen reduction reaction in acidic medium. Electrochim Acta 55:4403–4411
31. Liu H, Zhang J (2009) Controllable synthesis of porous carbon spheres, and electrochemical applications thereof. Patent WO2009/149540 A1
32. Zeng J, Francia C, Gerbaldi C, Dumitrescu MA, Specchia S, Spinelli P (2012) Smart synthesis of hollow core mesoporous shell carbons (HCMSC) as effective catalyst supports for methanol oxidation and oxygen reduction reactions. J Solid State Electrochem 16:3087–3096
33. Büchel G, Unger KK, Matsumoto A, Tsutsumi K (1998) A novel pathway for synthesis of submicrometer-size solid core/mesoporous shell silica spheres. Adv Mater 10:1036–1038
34. Jun S, Joo SH, Ryoo R, Kruk M, Jaroniec M, Liu Z, Ohsuna T, Terasaki O (2000) Synthesis of new, nanoporous carbon with hexagonally ordered mesostructure. J Am Chem Soc 122:10712–10713
35. Kruk M, Jaroniec M (2001) Gas adsorption of ordered organic-inorganic nanocomposite materials. Chem Mater 13:3169–3183
36. Jaroniec M, Solovyov LA (2006) Improvement of the Kruk–Jaroniec–Sayari method for pore size analysis of ordered silicas with cylindrical mesopores. Langmuir 22:6757–6760
37. Liu LiX, Ganesan P, Popov BN (2010) Studies of oxygen reduction reaction active sites and stability of nitrogen-modified carbon composite catalysts for PEM fuel cells. Electrochim Acta 55:2853–2858
38. Aricò AS, Antonucci V, Minutoli M, Giordano N (1989) The influence of functional groups on the surface acid–base characteristics of carbon blacks. Carbon 27:337–347
39. Zhu M, Weber CJ, Yang KM, Starke U, Kern K, Bittner AM (2008) Chemical and electrochemical ageing of carbon materials used in supercapacitor electrodes. Carbon 46:1829–1840
40. Shrestha S, Mustain WE (2010) Properties of nitrogen-functionalized ordered mesoporous carbon prepared using polypyrrole precursor. J Electrochem Soc 157:B1665–B1672
41. Subramanian NP, Kumaraguru SP, Colon-Mercado H, Kim H, Popov BN, Black T, Chen DA (2006) Studies on Co-based catalysts supported on modified carbon substrates for PEMFC cathodes. J Power Source 157:56–63
42. Shao Y, Zhang S, Engelhard MH, Li G, Shao G, Wang Y, Liu J, Aksay IA, Lin Y (2010) Nitrogen-doped graphene and its electrochemical applications. J Mater Chem 20:7491–7496
43. Kamiya K, Hashimoto K, Nakanishi S (2012) Instantaneous one-pot synthesis of Fe–N-modified graphene as an efficient electrocatalyst for the oxygen reduction reaction in acidic solutions. Chem Commun 48:10213–10215
44. Wang H, Maiyalagan T, Wang X (2012) Review on recent progress in nitrogen-doped graphene: synthesis, characterization, and its potential applications. ACS Catal 2:781–794
45. Gasteiger HA, Kocha SS, Sompalli B, Wagner FT (2005) Activity benchmarks and requirements for Pt, Pt-alloys, and non-Pt oxygen reduction catalysts for PEMFC. Appl Catal B Environ 56:9–35
46. Matter PH, Zhang L, Ozkan US (2006) The role of nano-structure in nitrogen-containing carbon catalysts for the oxygen reduction reaction. J Catal 239:83–96
47. Arrigo R, Havecker M, Schlogl R, Su DS (2008) Dynamic surface rearrangement and thermal stability of nitrogen functional groups on carbon nanotubes. Chem Commun 40:4891–4893
48. Niwa H, Horiba K, Harada Y, Oshima M, Ikeda T, Terakura K, Ozaki J, Miyata S (2009) Instantaneous one pot synthesis of Fe–N-modified graphene as an efficient electrocatalyst for the oxygen reduction reaction in acidic solutions. J Power Sources 187:93–97
49. Liu H, Shi Z, Zhang J, Zhang L, Zhang J (2009) Ultrasonic spray pyrolyzed iron-polypyrrole mesoporous spheres for fuel cell oxygen reduction electrocatalysts. J Mater Chem 19:468–470
50. van Veen JAR, Colijn HA, van Baar JF (1988) On the effect of a heat treatment on the structure of carbon-supported metalloporphyrins and phthalocyanines. Electrochim Acta 33:801–804
51. Bouwkamp-Wijnoltz AL, Visscher W, van Veen JAR, Tang SC (1999) Electrochemical reduction of oxygen: an alternative method to prepare active $CoN_4$ catalysts. Electrochim Acta 45:379–386
52. Liang C, Li Z, Dai S (2008) Mesoporous carbon materials: synthesis and modification. Angew Chemie Int Ed 47:3696–3717
53. Marcotte S, Villers D, Guillet N, Roué L, Dodelet JP (2004) Electroreduction of oxygen on Co-based catalysts: determination of the parameters affecting the two-electron transfer reaction in an acid medium. Electrochim Acta 50:179–188
54. Song C, Zhang J (2008) Electrocatalytic oxygen reduction reaction. In: PEM fuel cell electrocatalysts and catalyst layers, fundamental and applications, 1st edn. Springer, London, pp 89–134
55. Stassi A, D'Urso C, Baglio V, Di Blasi A, Antonucci V, Aricò AS, Castro Luna AM, Bonesi A, Triaca WE (2006) Electrocatalytic behaviour for oxygen reduction reaction of small nanostructured crystalline bimetallic Pt–M supported catalysts. J Appl Electrochem 36:1143–1149
56. Wang P, Ma Z, Zhao Z, Jia L (2007) Oxygen reduction on the electrocatalysts based on pyrolyzed non-noble metal/poly-*o*-phenylenediamine/carbon black composites: new insight into the active sites. J Electroanal Chem 611:87–95
57. Qiao J, Lin R, Li B, Ma J, Liu J (2010) Kinetics and electrocatalytic activity of nanostructured Ir–V/C for oxygen reduction reaction. Electrochim Acta 55:8490–8497
58. Zhang H-J, Yuan X, Sun L, Zeng X, Jiang Q-Z, Shao Z, Ma Z-F (2010) Pyrolyzed CoN4-chelate as an electrocatalyst for oxygen reduction reaction in acid media. Int J Hydrogen Energy 35:2900–2903
59. Pei K, Banham D, Feng F, Fürstenhaupt T, Ye S, Birss V (2010) Oxygen reduction activity dependence on the mesoporous structure of imprinted carbon supports. Electrochem Commun 12:1666–1669
60. Lai L, Potts JR, Zhan D, Wang L, Kok Poh C, Tang C, Gong H, Shen Z, Lin J, Ruoff RS (2012) Exploration of the active center structure of nitrogen-doped graphene-based catalysts for oxygen reduction reaction. Energy Environ Sci 5:7936–7942
61. Coutanceau C, Croissant MJ, Napporn T, Lamy C (2000) Electrocatalytic reduction of dioxygen at platinum particles dispersed in a polyaniline film. Electrochim Acta 46:579–588

62. Kapałka A, Foti G, Comninellis C (2008) Determination of the Tafel slope for oxygen evolution on boron-doped diamond electrodes. Electrochem Commun 10:607–610
63. Li S, Zhang L, Kim J, Pan M, Shi Z, Zhang J (2010) Synthesis of carbon-supported binary FeCo–N non-noble metal electrocatalysts for the oxygen reduction reaction. Electrochim Acta 55:7346–7353
64. Wang L, Zhang L, Zhang J (2011) Optimizing catalyst loading in non-noble metal electrocatalyst layer to improve oxygen reduction reaction activity. Electrochem Commun 13:447–449